MINISTRY OF EDUCATION AND TRAINING

VIETNAM ACADEMY OF SCIENCE AND TECHNOLOGY

GRADUATE UNIVERSITY OF SCIENCE AND TECHNOLOGY

Le Van Long

RESEARCH ON CONTROLLING ELECTROMAGNETIC WAVE ABSORPTION CHARACTERISSTICS OF METAMATERIALS BY MECHANICAL IMPACT AND VOLTAGE

SUMMARY OF DISSERTATION ON MATERIALS FOR ELECTRONICS

Code: 9 44 01 23

Hanoi - 2024

The dissertation is completed at: Graduate University of Science and Technology, Vietnam Academy Science and Technology

Supervisors:
Supervisor 1: Dr. Bui Son Tung, Graduate University of Science and Technology, Vietnam Academy Science and Technology.
Supervisor 2: Prof. Dr. Vu Dinh Lam, Graduate University of Science and Technology, Vietnam Academy Science and Technology.

Referee 1:.....

Referee 2:.....

Referee 3:.....

The dissertation will be examined by Examination Board of Graduate University of Science and Technology, Vietnam Academy of Science and Technology at…….. (time, date……)

The dissertation can be found at:

1. Graduate University of Science and Technology Library
2. National Library of Vietnam

INTRODUCTION

1. The urgency of the dissertation

The history of engineered metamaterials (MM) involves key contributions from Jagadis Chunder Bose, Karl F. Lindman, and Winston E. Kock. Victor Veselago introduced the MM concept in 1968, leading to research on materials with negative refractive indices. John Pendry and David R. Smith further advanced MM through modeling and experiments. MM research has yielded applications in optics, telecommunications, sensors, and energy harvesting. Metamaterial absorbers (MA) are notable for their ability to absorb waves across various frequencies, enabling applications in energy, stealth, sensors, and communications. However, traditional MAs struggle to adjust frequency and absorption intensity. In Vietnam, MA research has focused on optimizing absorption but not on controlling properties via external effects. Hence, the project "*Research on controlling electromagnetic wave absorption characteristics of metamaterials by mechanical impact and voltage*" aims to enhance MA's practical applications by enabling property control through external impacts.

2. Research objectives of the dissertation

- Design and fabricate MMs capable of controlling electromagnetic wave absorption properties by mechanical impact and voltage.
- Clarifying the absorption mechanism and the change in electromagnetic wave absorption properties of MM under external impact.

3. Research method of the dissertation

- The dissertation is based on a combination of calculation, simulation, fabrication and experimental measurements.
- Electromagnetic properties such as reflection, transmission and absorption of the material will be simulated and compared with calculation results. Then, based on the theoretical results, the MM sample will be fabricated based on the photolithography technique. Finally, the electromagnetic properties of

MM will be measured by a vector network analyzer.

4. Research contents and new contributions of the dissertation

- The dissertation has successfully designed and fabricated MM structures capable of actively controlling electromagnetic wave absorption properties by simple mechanical impacts such as rotation, pulling and bending.
- The absorption mechanism and the principle of controlling absorption properties by mechanical impact have been clarified.
- The dissertation has successfully designed MM structures capable of actively controlling electromagnetic wave absorption characteristics using external voltage.
- The dissertation has fabricated a multifunctional MM that can be controlled by external voltage, allowing flexible conversion from the function of absorbing electromagnetic waves to the function of rotating the polarization angle of electromagnetic waves.
- Analyzed the operating mechanism of MMs controlled by external voltage.

The dissertation includes an introduction, 4 content chapters and a conclusion.

Chapter 1. OVERVIEW OF METAMATERIALS CONTROLLED BY EXTERNAL IMPACTS

1.1. Electromagnetic metamaterial absorber and operation principle

1.1.1. Electromagnetic characteristics of metamaterials based on the resonance phenomenon

Artificial composite materials like metamaterials (MM) are made by designing small cell structures, or artificial atoms, that are smaller than the wavelength. This creates a uniform medium with adjustable electromagnetic properties based on effective medium theory. MM can surpass the limitations of conventional materials. The unit-cell structures, often resonant, such as metal wires or LC and dielectric structures, are designed to produce desired electromagnetic characteristics. Utilizing resonance, MM can create diverse

electromagnetic properties, including metamaterial absorbers (MA).

1.1.2. Electromagnetic metamaterial absorber and structural classification

The design of the MA structure can be classified into several basic types such as: Metal-dielectric-metal three-layer structure, Metal-only structure and Metal-dielectric two-layer structure.

1.2. The principle of controlling the electromagnetic properties of metamaterials by external impacts

1.2.1. Control the electromagnetic properties of metamaterials by mechanical impact

By integrating an actuator, the thickness of the air dielectric layer of the MA sample is controlled. The results show that the absorption frequency of MA shifts with the absorption frequency control level of 0.12 GHz/

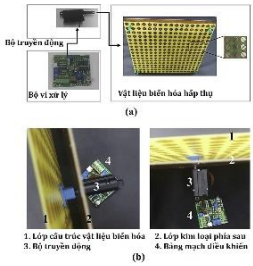

Figure 1.10. (a) Block diagram of MA integrated with the actuator. (b) Magnified image.

1.2.2. Control the electromagnetic properties of metamaterials by external voltage

Yang Liu designed a controllable MA by external voltage using variable capacitance diodes. When changing the external voltage, the absorption frequency range and absorption of MA change due to the variation in capacitance value of the diode.

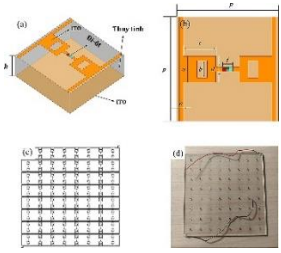

Figure 1.14. (a) Unit cell of MA. (b) Top view of the unit cell. (c) Model and (d) sample photos of MA.

1.2.3. Control the electromagnetic properties of metamaterials by external magnetic field

MA is controlled by an external magnetic field, using a ferrite block from yttrium iron garnet (YIG) placed on a copper plate.

Measurement results show that the high absorption is maintained stably, and the absorption spectrum of MA can be controlled to shift toward high frequencies when the external magnetic field intensity increases.

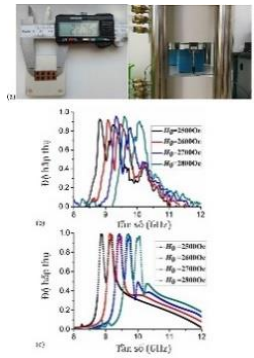

Figure 1.22. (a) MA sample and electromagnet. (b) Measured and (c) simulated absorption spectra under different magnetic fields.

1.2.4. Control the electromagnetic properties of metamaterials by temperature

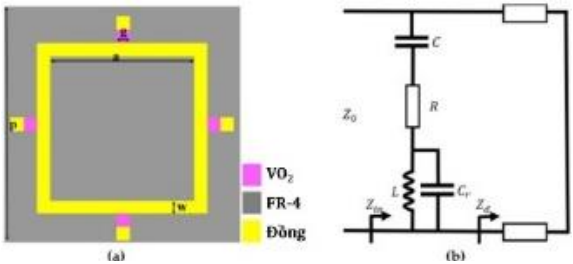

Figure 1.26. (a) Design of metal/dielectric/metal structured MA integrated with VO_2 and (b) equivalent circuit model.

The proposed thermally-controlled MA is based on the phase change material vanadium dioxide (VO_2). The MA gives a reflection minimum at 7.1 GHz at room temperature. After VO_2 change its phase, this minimum shifts to 6.3 GHz. The increase in inductance in the metallic phase has caused the resonance to shift towards lower frequencies.

1.2.5. Control the electromagnetic properties of metamaterials by optics

MA has the ability to actively control through optical stimulation on the carrier in GaAs to dynamically control the response of electrical split-ring resonator (eSRR) structures on the GaAs buffer layer. Under the condition of no incident beam, two resonances appear at 0.78

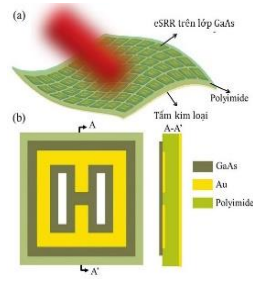

Figure 1.31. (a) Optically controllable MA and (b) unit cell of MA (top and cross-section).

THz (80% absorption) and 1.75 THz (99% absorption). When there is an incident beam and increasing power, the dual-band absorption spectrum decreases and changes to a single-peak absorption spectrum at 0.95 THz.

1.3. Potential applications of electromagnetic metamaterial absorber controlled by mechanical impact and voltage

1.3.1. Applications of electromagnetic metamaterial absorber controlled by mechanical impact

Using the 3D printing method, the force sensor based on MA was made of flexible plastic and conductive ink. When subjected to pressure up to 20 N, the resonant frequency changes from 5.2 GHz to 5.66 GHz. The proposed pressure sensor exhibits a sensitivity of 7.75×10^8 Hz/mm (0.2×10^8 Hz/N) and stable performance over 100 cycles.

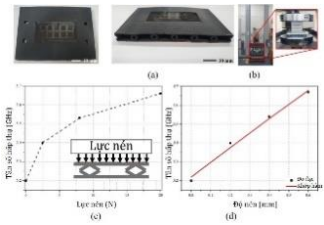

Figure 1.35. (a) MA-based force sensor. (b) Model and measurement results of the variation of absorption frequency according to (c) compression force and (d) compression degree.

1.3.2. Applications of electromagnetic metamaterial absorber controlled by external voltage

A MA sample is made up of a CW resonance structure on a polyimide layer and a bottom layer of carbon fiber/epoxy composite material. The integrated variable diode between the CWs, can adjust the capacitance as the voltage changes. By placing the structures in the shape of the number "8" and independently controlling the voltage, the thermal image of the digits "2", "3", "5", "6", "8", and "9" appeared.

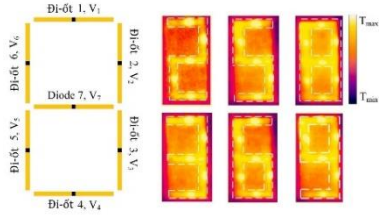

Figure 1.38. Displays thermal images of the digits.

Chapter 2. RESEARCH METHODS

2.1. Calculation method of electromagnetic metamaterials

2.1.1. Equivalent circuit model

The resonant frequency of the MM can be calculated based on the LC equivalent circuit model, in which the metallic and dielectric components will contribute to the effective L and C values of the equivalent circuit.

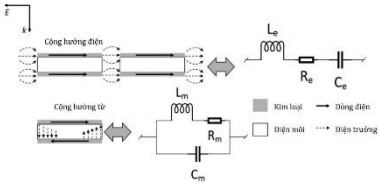

Figure 2.2. Current and electric field distributions are simplified, and the equivalent circuit model of the CWP at electric and magnetic resonance modes.

2.1.2. Impedance of metamaterial

For MA, transmission is typically eliminated with a continuous metal plate, while reflection is minimized through impedance matching. If the real part of the MA impedance is about 1 and the imaginary part is about 0, incident electromagnetic waves are not reflected. The impedance of MA can be calculated by the formula: $Z(f) = \sqrt{\frac{[1+S_{11}(f)]^2-[S_{21}(f)]^2}{[1-S_{11}(f)]^2-[S_{21}(f)]^2}}$.

Besides the above method, MA impedance can also be calculated using the transmission line theory (TL) model. The front resonant structure (FSS) acts as a resonant circuit with impedance Z_{FSS}. The dielectric substrate and the continuous metal layer (GND) form a short-circuit transmission line with impedance Z_d, calculated using the dielectric thickness h and permittivity ϵ_d according to the formula: $Z_d = i\frac{Z_0}{\sqrt{\varepsilon_d}}\tan\left(k_0\sqrt{\varepsilon_d}h\right)$,

where, Z_0 and k_0 are the impedance and wavenumber of the air. Then, the impedance of MA, denoted Z_T, is considered as a parallel combination of two impedance components Z_{FSS} and Z_d: $Z_{\mathrm{T}} = Z_{FSS}//Z_d = \frac{Z_{FSS}Z_d}{Z_{FSS}+Z_d}$.

2.2. Simulation method of electromagnetic metamaterials

2.2.1. CST Microwave simulation software

CST MWS is one of the commercial 3D electromagnetic simulation software,

based on finite integration technique (FIT), specialized in designing and researching the electromagnetic properties of materials, components and electronic equipment, including MM.

2.2.2. Structure design

MM design involves selecting materials (metals, dielectrics) and components (capacitors, diodes) with specific electromagnetic parameters. The unit cell's geometrical structure is then designed, followed by applying periodic boundary conditions to ensure the simulated material matches the actual material.

2.2.3. Simulate and analyze the electromagnetic characteristics of metamaterials

After simulation, CST software calculates electromagnetic scattering parameters, including reflection and transmission components. From these, wave absorption and polarization conversion ratios can be determined. The software advantageously simulates physical phenomena such as current distribution, electric and magnetic fields, and energy loss, clarifying the material's operating mechanism.

2.3. Fabrication method of electromagnetic metamaterials

To fabricate MA samples operating in the GHz region, a photolithography fabrication system is used, including key components such as illumination, metal etching, and photosensitive cleaning.

2.4. Measurement method of electromagnetic properties of metamaterials

In the GHz region, the equipment to measure the interaction of electromagnetic waves with materials is the Rohde & Schwarz ZNB20 vector network analyzer system connected to two antennas, which play the role of transmitting and receiving signals of traveling waves.

Figure 2.18. Image of vector network analyzer used to measure the electromagnetic properties of MA.

Chapter 3. CONTROL THE ELECTROMAGNETIC WAVE ABSORPTION CHARACTERISTICS OF METAMATERIALS BY MECHANICAL IMPACT

3.1. Controlling the electromagnetic wave absorption frequency range in the GHz region by rotating the relative positions between layers of the metamaterial

3.1.1. Multi-layer-metamaterial structure

The structure consists of five layers: copper ring metal layer, GCI ring metal layer, and continuous copper layer on the back; Polyimide dielectric layers of 0.5 and 1 mm thickness are located between the metal layers. The thickness of the metal layer is 0.036 mm, and the copper material has an electrical conductivity of 5.96×10^7 S/m, while GCI has a resistance of 6.5 ohm/sq.

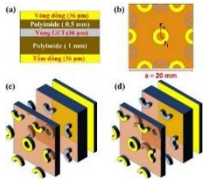

Figure 3.1. Design of multilayer MA. (a) side view, (b) front view in CRC configuration, (c) three-dimensional models of CRC and (d) MRC configurations.

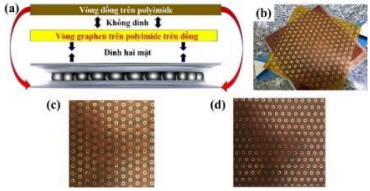

Figure 3.2. (a) Reconfigurable multilayer MA diagram placed on a turntable bearing (b) during rotation, (c) after rotation in CRC configuration, and (d) after rotation in MRC configuration.

The polyimide dielectric layer has a dielectric constant of 3.5 and a loss tangent of 0.0027. The rings have an outer radius r_o = 2.5 mm and an inner radius r_i = 1.5 mm, forming a hexagon around the central ring. The top layers can be rotated to switch between matched ring configuration (MRC) and crossed ring configuration (CRC). The MA can be controlled mechanically, rotating the turntable to switch between two configurations. The image of the

fabricated MA sample and the stacking position after rotation are shown in Figure 3.2.

3.1.2. Control the absorption frequency range of the metamaterial by changing the relative position between the layers

For MRC, the absorption peak reaches almost 80% at 13.7 GHz with a small shoulder at 12.8 GHz in both TM and TE modes. Rotating the upper layer 90° to form CRC significantly enhances absorption, reaching 100% at 11.5, 12.1, and 13.5 GHz, and over 95% at 14.1 GHz in TE mode.

In TM mode, absorption at 14.1 GHz decreases slightly, but the peak at 15.1 GHz rises from below 80% to 94%. This change from MRC to CRC enhances absorption intensity and broadens the absorption frequency range, doubling it for 50% absorption and improving it by 360% (TE) and 469% (TM) for 70% absorption.

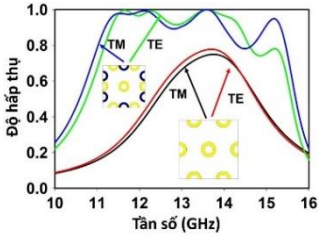

Figure 3.3. Simulated absorption spectra of MA correspond to two configurations, MRC and CRC, when the incident electromagnetic waves are polarized in TE and TM modes.

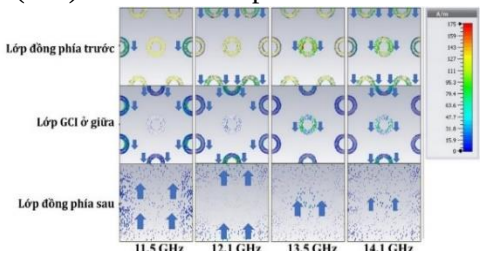

Figure 3.5. Induced currents on the layers of MA when the electromagnetic wave is polarized in TE mode.

At 11.5 GHz, the current on the bottom copper layer concentrates around the vertical edges of the unit cell, antiparallel to the current on the GCI and copper rings, indicating magnetic resonance. This pattern is similar for peaks at 12.1, 13.5, and 14.1 GHz but varies in current position: at 12.1 GHz, it is on the horizontal edges; at 13.5 GHz, at the center; and at 14.1 GHz, at both the central and horizontal resonant rings.

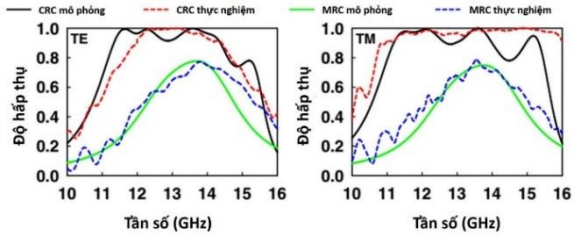

Figure 3.9. Simulated and measured absorption spectra in CRC and MRC configurations in (left) TE and (right) TM modes.

Experimental results align well with simulations. Rotating the MA layers enhances and broadens absorption in the CRC configuration compared to MRC. Absorption peaks at 11.5 and 15.1 GHz in TE mode slightly reduce, and peaks from 12-14.5 GHz merge. In TM mode, the measured absorption spectrum matches the simulated one, showing good broadband performance. Differences may arise from the practical complexity of rotating multilayer samples and slight inhomogeneities in the fabricated GCI rings. Nonetheless, MA effectively converts between single-peak and broadband absorption modes through mechanical adjustments.

3.2. Controlling electromagnetic wave absorption in the GHz region by mechanically transforming the shape of the metamaterial structure based on origami technique

3.2.1. Design of paper metamaterial

Origami-Based Metamaterial (OBMM) is designed as a multifunctional MM that can alter its structure. It's crafted from paper with a surface layer of conductive ink and a copper layer underneath. The OBMM design comprises two layers: a periodic structure printed on paper with conductive ink and a metal layer. The paper acts as a dielectric with thickness t_d, featuring ε_r = 2.85 and ε_i = 0.035. The conductive ink, with conductivity σ, is used to optimize absorption capacity along with thickness t_m.

The ink conductivity is adjusted to study OBMM absorption properties. Beneath is a continuous copper layer with conductivity 5.8×10^7 S/m and thickness t_s=0.036 mm. The unit-cell size in both x and y axes is a=10 mm.

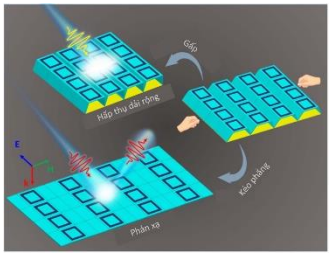

Figure 3.10. Illustration of two modes: absorption and reflection using origami MM.

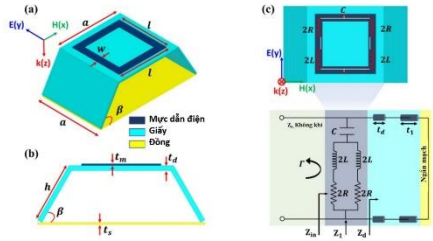

Figure 3.11. (a-b) Schematic of the designed unit cell with structural parameters and (c) corresponding TL equivalent circuit.

The structure's shape depends on the tilt angle β, which affects unit cell height and size. Following the auxetic property, as β increases, the x-axis size decreases. The printed structure is a square ring with side length l=8 mm and width w=1.5 mm. Paper, printing structure, and copper layer thicknesses are t_d=0.254 mm, t_m=0.05 mm, and t_s=0.036 mm, respectively. The inclined paper length h is 6 mm, and ink conductivity is σ=700 S/m.

3.2.2. Controlling the absorption of metamaterial using origami paper folding technique

In folding mode (Mode I), OBMM functions as an absorber, while in flat stretching mode (Mode II), it acts as a reflector. In Mode I, with a tilt angle β of 90°, simulation achieves over 95% absorption across a wide frequency range from 5.5 to 16 GHz. TL circuit calculations show consistent results, with absorption exceeding 90% from 7 GHz to over 20 GHz. Conversely, flattening the structure horizontally creates an entirely reflective configuration (Mode II). Simulation and calculation confirm nearly zero absorption, as the incident wave is fully reflected by the copper layer.

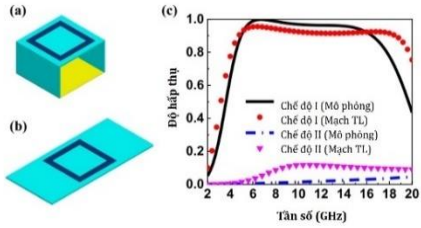

Figure 3.12. Structural configuration in (a) mode I and (b) mode II. (c) Corresponding absorption spectra in comparison between simulation and TL equivalent circuit calculation.

At absorption peaks, current concentrates on the front square ring's longitudinal edges in the E direction, while evenly spread on the rear copper plate. At 15.1 GHz, current distribution between layers is parallel, but antiparallel at 5.8 GHz. This occurs due to interaction between the printed square ring structure and the copper layer. When excited by incident electromagnetic waves, the structure behaves similarly to a cut-wire pair MM, resulting in two resonant frequencies: one causing antiparallel current distribution (magnetic resonance) and another causing parallel current distribution (electrical resonance).

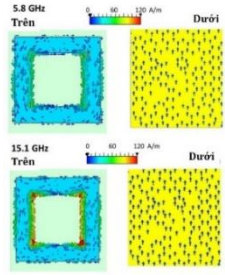

Figure 3.13. Simulated current distributions in mode I at 5.8 GHz and 15.1 GHz.

Therefore, the absorption peak at 5.8 GHz can be explained by the appearance of magnetic resonance, while the absorption peak at 15.1 GHz is caused by electrical resonance. Next, the dissertation investigates the change in the absorption properties of the OBMM structure by changing the values of σ and h to consider their influence on the frequency and absorption band. The absorption band reached the optimal value of 117% with conductivity and ink layer thickness of σ = 700 S/m and t_m = 0.05 mm, respectively. Besides, when the value of h increases from 6 to 8 mm, the maximum absorption of the proposed structure reaches over 90% in all cases β = 90°, 70° and 50°. When h is equal to 5 mm, both the bandwidth and the maximum absorption value decrease as β decreases.

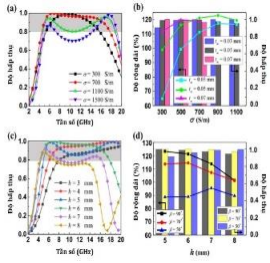

Figure 3.14. Absorption characteristics under different values of (a) ink conductivity σ and (b) length h. Optimal values of band gap and absorption intensity according to (c) conductivity σ and thickness t_m of the structure,

In addition, the proposed OBMM structure does not depend on the polarization angle φ due to the symmetry in the structure and strong attenuation when the incident angle θ is large from 60° or more.

3.3. Controlling the frequency range of electromagnetic wave absorption in the THz region by bending the metamaterial

3.3.1. Design of bendable electromagnetic metamaterial absorber in the THz region

The MA design model in the bendable THz region (Figure 3.17) comprises three main parts: a continuous metal layer at the bottom, a continuous dielectric layer in the middle, and a discontinuous metal layer on top forming resonance structures. Each unit cell includes a central slotted plus (SP) resonant structure and four slotted plus ring resonator (SRR) structures symmetrically positioned at the corners. Geometric parameters are detailed in Table 3.2. For simulation, polyimide (permittivity 3.5 with a loss tangent of 0.0027) and silver (conductivity 6.3×10^7 S/m) are used as dielectric and metallic materials, respectively.

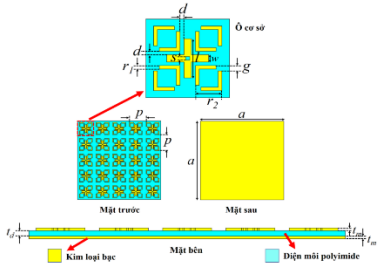

Figure 3.17. MA design in the THz region.

Table 3.2. Values of the structural parameters of the simulated MA.

Structural parameters	Symbol	Value (µm)
Size of MA	a	1100
Dielectric layer thickness	t_d	2
Metal layer thickness	t_m	0,2
Size of the unit cell	p	220
Length of SP	l	110
Width of SP	w	20
Size of slot on SP	s	10
Distance between SP and SRR	d	5
Size of SRR	r_1	10

Width of SRR	r_2	70
Square-slot size of SRR	g	15

3.3.2. Control the absorption frequency range of the metamaterial by bending

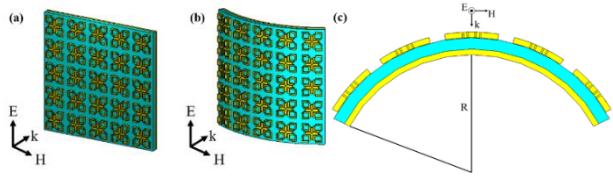

Figure 3.23. (a) MA in flat state, (b) MA in bent state, (c) Define the degree of bending of the MA according to the bending radius R.

In the flat state, MA exhibits three absorption peaks around 0.76, 0.91, and 0.94 THz, each exceeding 90% absorption. When R = 1000 µm, five absorption peaks emerge at frequencies around 0.76, 0.81, 0.89, 0.92, and 0.93 THz, with corresponding absorbances of 95%, 91%, 92%, 95%, and 99%. At R = 750 µm, two absorption peaks appear at 0.74 and 0.82 THz, with absorption values of 99.8% and 95%, respectively. Combining higher frequency peaks creates a seamless absorption band from 0.88 to 0.93 THz, maintaining absorption above 90%. At R = 500 µm, absorption at peaks around 0.75 and 0.82 THz is reduced, yet a wide absorption band from 0.86 to 0.96 THz persists with absorption exceeding 90%.

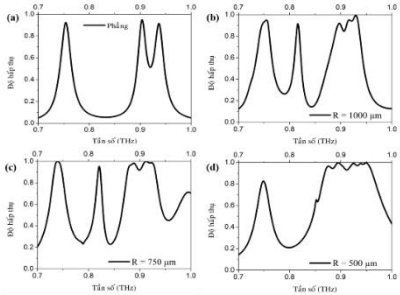

Figure 3.24. Simulated absorption spectra of MA with dielectric layer thickness t_d = 10 µm in flat and bent states with different bending radii R.

3.4. Conclusions of chapter 3

- Designed and fabricated a multilayer MA that can control between single-peak absorption and broadband absorption by mechanically rotating the structural layers of the MA. It has been clarified that the control mechanism

is due to the mechanical rotation action that reconfigures the material and creates different structures of MA.

- Designed a simple MA made from paper that can be switched between broadband absorption and reflection by folding or stretching. It has been clarified that the control mechanism is due to the reconfigured folding or stretching action that creates or destroys the dielectric layer of the MA.
- Designed MA in the THz region with the absorption frequency range controlled by bending the MA.
- Investigated and evaluated the electromagnetic properties of the proposed MAs under the influences of structural parameters as well as the incidence angle and polarization angle of electromagnetic waves.

Chapter 4. CONTROL THE ELECTROMAGNETIC WAVE ABSORPTION CHARACTERISTICS OF METAMATERIALS BY EXTERNAL VOLTAGE

4.1. Multifunctional metamaterial capable of switching between the absorption function and the function of rotating the polarization angle of electromagnetic waves in the GHz region

4.1.1. Multifunctional metamaterial structure

The MM structure comprises three layers: a polyimide dielectric layer sandwiched between two copper layers (Figure 4.1(a)). The dielectric layer has a constant of 3.5 and a loss tangent of 0.0027. The copper layers have a conductivity of 5.8×10^7 S/m. The continuous bottom copper layer prevents EM wave passage, while the top layer features periodic split-ring resonator structures and DC power supply lines. Two power supply

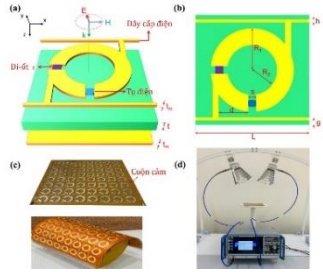

Figure 4.1. (a) Schematic diagram of the proposed MM unit cell structure. (b) Top view of the unit cell with structural parameters: L = 24.5, R_1 = 10, R_2 = 5.8, s = 1, d =

lines feed voltage to variable diodes in each unit cell. Capacitors with fixed capacitance values at the bottom ring gap create a highly anisotropic structure in the DPC state. A capacitor with a capacitance of 0.2 pF is used to create the multifunctional MM. The diode used has the model number SMV2019-079LF, with a capacitance varying from 2.31 to 0.24 pF when the reverse DC bias voltage supplied through the supply lines varies from 0 to -19 V.

8.5, g = 0.5, h = 0.5, t = 2, t_m = 0.035 mm. (c) Fabricated MM sample with integrated capacitors and diodes and (d) absorption measurement configuration using a ZNB20 vector network analyzer.

Table 4.1. Effective parameter values of the diode.

VR (V)	***C* (pF)**	***R* (Ω)**	***L* (nH)**
0	2,31	4,51	0,7
-4	0,84	4,04	0,7
-7	0,55	3,66	0,7
-11	0,38	3,18	0,7
-14	0,31	2,86	0,7
-16	0,27	2,.65	0,7
-19	0,24	2,38	0,7

4.1.2. Switch between the function of absorbing electromagnetic waves and the function of rotating the polarization angle of electromagnetic waves by external voltage

In the first state with 0 V applied voltage, the MM operates in a single-peak absorption (SPA) state, resonating at 3.84 GHz. The co-reflection coefficient remains extremely small at 0.03, with a cross-reflection coefficient around 0.3 at this frequency. Absorption peaks near 3.85 GHz exhibit close to 90% absorption. Applying a bias voltage of approximately -19V induces a dual polarization-conversion (DPC) state. At the resonant frequencies of 4.59 GHz and 4.86 GHz, cross-reflection coefficients reach 0.9 and 0.91, respectively, with co-reflections around 0.04 and 0.02.

Reflected waves at these frequencies are nearly linearly polarized, with a rotation of 90 degrees compared to incident wave polarization. The polarization conversion ratio (PCR) exceeds 80% across a wide frequency range from 4.54 to 4.9 GHz, with PCR values near 100% at resonant frequencies. Experimental resonant frequencies measure approximately 4.6 and 5 GHz, with PCR coefficients of 96% and 92%, respectively.

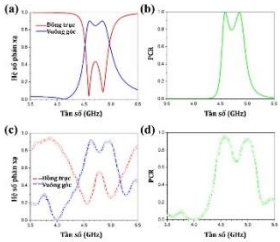

Figure 4.3. (a) Simulated co- and cross-reflection coefficients and (b) corresponding PCR coefficients of MM at bias voltage -19 V. Measurement results at -19 V of (c) reflection coefficients and (d) PCR coefficient, respectively.

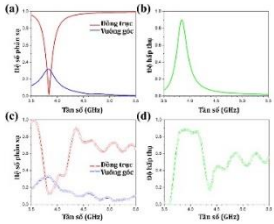

Figure 4.2. (a) Simulated co- and cross-reflections and (b) simulated absorption of MM at 0 V bias voltage. Measurement results at 0 V of (c) reflection coefficient and (d) absorption.

4.2. Control the frequency of electromagnetic wave absorption using voltage based on peripheral components integrated into the metamaterial

4.2.1. Design of metamaterial capable of controlling absorption frequency by external voltage

The unit-cell designs of single-band and dual-band MAs are illustrated in Figure 4.8. These MAs consist of a periodic array of unit cells arranged in the corresponding sample plane. Essentially, both types of MAs consist of three layers: a continuous metal back plate, a middle continuous dielectric layer, and a front metal structure with integrated inductors and diodes. For single-band MA, the unit cell uses a symmetric four-split ring resonator (s-SRR) structure with two capacitive diodes integrated in two gaps to control the resonance frequency of the structure. Metal power-supply lines are

designed at the top and bottom of the s-SRR, DC voltage is applied to the variable diodes. To prevent microwave signals from interfering with the DC

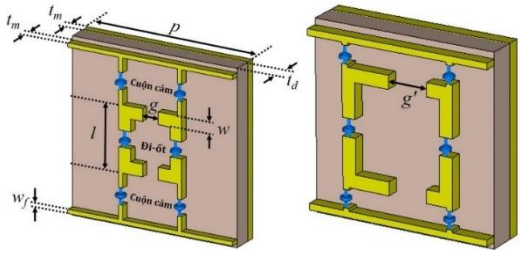

(a) (b)

Figure 4.8. Unit-cell structures of (a) single-band and (b) dual-band MAs.

bias, an inductor is placed between the power supply line and the s-SRR. The design of the dual-band MA follows a similar approach. However, the top and bottom gaps of the resonance structure is widened toward the right, creating an asymmetric four-split ring resonator structure (a-SRR). The middle dielectric layer is FR-4 with a relative dielectric constant of 4.3 and a loss of 0.025. Copper with an electrical conductivity of 5.8×10^7 S/m was chosen as the material used for both the front and rear layers. The inductance of the AC inductor is 100 µH. To control the electromagnetic properties of MA, variable diode SMV2019-079LF is selected.

Table 4.2. Structural parameters of single-band MA.

p (mm)	t_d (mm)	t_m (mm)	l (mm)	w (mm)	g (mm)	w_f (mm)
21	2,4	0,035	8	1,5	2	0,5

Table 4.3. Structural parameters of dual-band MA.

p (mm)	t_d (mm)	t_m (mm)	l (mm)	w (mm)	g (mm)	g' (mm)	w_f (mm)
14,6	2,2	0,035	9	1,05	2	3,1	0,5

4.2.2. Control the absorption frequency of the metamaterial by external voltage

Initially, in the absence of voltage applied to the variable diode, the MA obtained a prominent absorption peak in the C band at 4.7 GHz with an

absorption of 91%. When a -4V bias voltage is applied, a noticeable change occurs as the absorption peak shifts to a higher frequency of 5.4 GHz. At the same time, the absorption intensity increased significantly, reaching a value of 99%. Then, by gradually increasing the bias voltage, the absorption peak of MA continues to blue-shift. Specifically, at the bias voltages -7V, -14V and -19V, the corresponding absorption frequencies are 5.7 GHz, 6.1 GHz and 6.4 GHz, respectively.

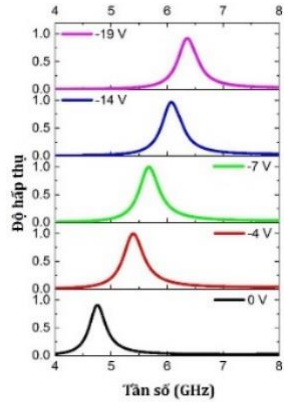

Figure 4.9. Dependence of absorption spectrum of single-band MA on external voltage.

Notably, despite the change in the absorption peak position, the absorption intensity is still relatively high, with values of 99%, 97% and 92%, respectively. This means that the MA maintains its absorption capacity effectively, even when the bias voltage changes. These results contribute to opening up the potential application of absorption control in the C band of the proposed MA structure. To better understand the absorption characteristics during external voltage changes, the induced current on the MA was simulated under two separate conditions: 0V and -19V.

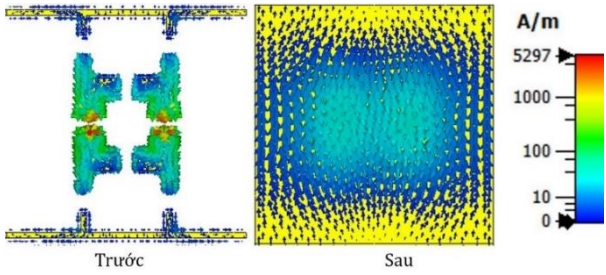

Figure 4.10. Surface current distributions on MA at the absorption frequency of 4.7 GHz corresponding to an applied voltage of 0V.

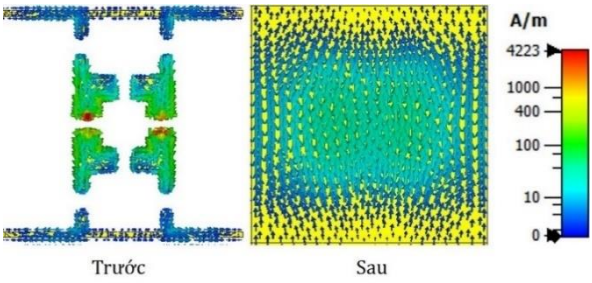

Figure 4.11. Surface current distributions on MA at the absorption frequency of 6.4 GHz corresponding to an applied voltage of 19 V.

In both cases, the induced currents in the front and back copper layers are antiparallel, showing that magnetic resonance occurs at the absorption frequency. In addition, the currents are mainly concentrated in the regions corresponding to the positions of the s-SRRs, demonstrating that the magnetic resonance is mainly generated by the s-SRR structure, while the influence of the power supply line is negligible.

Based on the asymmetry of the resonance structure, a-SRR obtains two distinct absorption peaks when no voltage is applied. The first peak was observed at 4.7 GHz with 95.8% absorption, while the second peak appeared at 5.6 GHz with 91.5% absorption. When applying a voltage of -4V, the absorption spectrum shifts to a higher frequency region. Therefore, the first and second absorption peaks reach 99.8% and 90% at frequencies of 5.2 GHz and 5.8 GHz, respectively. The blue-shift tendency persists when increasing the external voltage. Notably, the dual-band MA maintains over 90% absorption throughout the adjustment process even when the external voltage is up to -14V.

However, for an applied voltage of -19V, the absorption of the first peak decreased slightly to 81.6%, while the absorption of the second peak remained high.

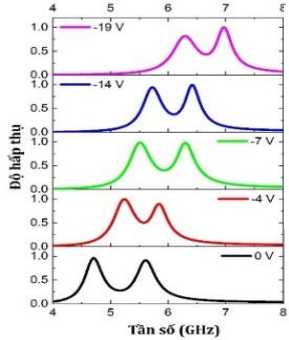

Figure 4.12. Dependence of absorption spectrum of dual-band MA on external voltage.

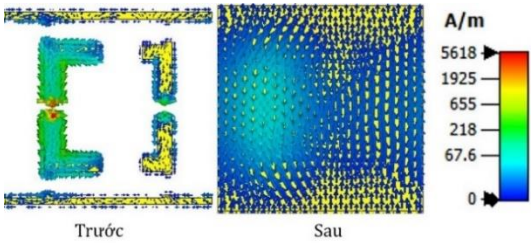

Figure 4.13. Surface current distributions on MA at the first absorption frequency of 4.7 GHz corresponding to an applied voltage of 0V.

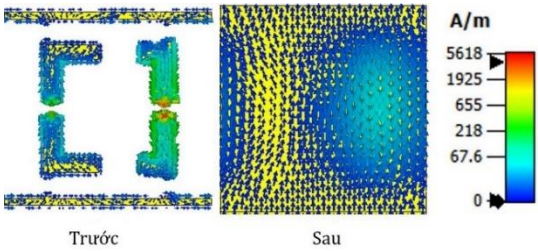

Figure 4.14. Surface current distributions on MA at the second absorption frequency of 5.6 GHz corresponding to an applied voltage of 0V.

Similar to the observation in single-band MA, the induced currents in the front and back metal layers are antiparallel at both resonant frequencies, which confirms the magnetic resonance excitation giving rise to the absorption peak. Notably, at the first resonant frequency, the currents are mainly concentrated in regions corresponding to the left section of a-SRR, while at the second resonant frequency, they are mainly concentrated in regions corresponding to the right section of a-SRR.

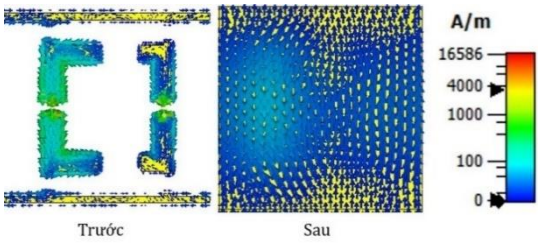

Figure 4.15. Surface current distributions on MA at the first absorption frequency of 6.3 GHz corresponding to an applied voltage of -19V.

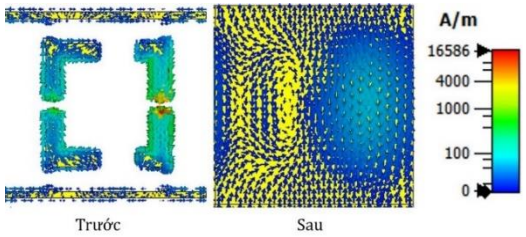

Figure 4.16. Surface current distributions on MA at the second absorption frequency of 6.9 GHz corresponding to an applied voltage of -19V.

4.3. Conclusions of chapter 4

- Designed and fabricated a multifunctional MM controlled by external voltage. The absorption function and polarization angle rotation function of the electromagnetic wave can be switched by changing the voltage on the diode integrated in the MM. The control mechanism is due to the symmetry axis of the MM structure changes when the properties of the diode change with voltage.
- Designed and simulated single- and dual-band MAs capable of controlling the absorption frequency by voltage in the C band. The control mechanism is due to the effective capacitance of the MA changes when the properties of the diode change with voltage, resulting in the LC resonance frequency being shifted.

CONCLUSIONS AND RECOMMENDATIONS

The dissertation *"Research on controlling electromagnetic wave absorption characteristics of metamaterials by mechanical impact and voltage"* was carried out at the Graduate University of Science and Technology and the Institute of Materials Science, Vietnam Academy of Science and Technology. The main research results of the dissertation have been published in 03 international journal articles under the SCIE category, 01 national journal article and 01 conference proceedings, specifically including:

The dissertation contributes to research on Materials Science in general and Metamaterials in particular. Some main specific research results are as follows:

1. Successfully designed and fabricated MA that can control absorption properties by mechanical rotation. In its initial state, the MA has an MRC configuration giving 80% absorption at 13.7 GHz. When the top layer is rotated 90°, the MA switches to a CRC configuration for broadband

absorption with the frequency range corresponding to absorption above 70% being 360% wider, in TE mode, and 469% wider, in TE mode. TM degree compared to MRC configuration.

2. An OBMM has been designed that can control the absorption properties by streching action. When MA is streched flat, OBMM reflects the incoming electromagnetic wave. When the MA is folded, the OBMM absorbs incoming electromagnetic waves in a wide range from 5.5 to 16 GHz.

3. Successfully designed and fabricated a BMM that can be controlled by external voltage. When there is no external voltage, the BMM operates in absorption function with 90% absorption at 3.85 GHz. When an external voltage of 19 V is applied, the BMM switches to a dual-band polarization conversion function with a polarization conversion ratio of 96% and 92% at 4.6 and 5 GHz, respectively. At these two frequencies, the electromagnetic wave incident on the BMM will mostly be reflected with the polarization angle of the reflected wave rotated 90° compared to the polarization angle of the incident wave.

The results achieved by the dissertation can make an important contribution to the development of future smart devices related to electromagnetic wave shielding and radar or in the fields of communication. These results also contribute to the development of multifunctional devices, based on active control of the electromagnetic properties of MM.

Further research directions, extending to higher frequency regions, such as the infrared and optical regions, will be an important next step. Exploiting the absorption properties of MMs in these frequency ranges could lead to novel applications in the fields of optical communications, signal processing and also in the field of medicine, where high frequencies can provide detailed information about molecular and cellular structures.

In summary, research on controlling the absorption amplitude and frequency of modified materials is not only opening up promising application

prospects, but also provides a foundation for further research on integrating them into smart electronic devices and explore new applications in higher frequency ranges.

LIST OF THE PUBLICATIONS RELATED TO THE DISSERTATION

1. **Le Van Long**, Dinh Ngoc Dung, Pham Thanh Son, Nguyen Thanh Tung, Vu Thi Hong Hanh, Duong Thi Ha, Do Thuy Chi, Bui Son Tung, Bui Xuan Khuyen, and Vu Dinh Lam, "*Robust reversion of dual-band polarization conversion and absorption based on flexible metamaterial*", Journal of the Physical Society of Japan **92**, 024801 (2023).

2. **Le Van Long**, Nguyen Hoang Tung, Trinh Thi Giang, Pham Thanh Son, Nguyen Thanh Tung, Bui Son Tung, Bui Xuan Khuyen, and Vu Dinh Lam, "*Rotary bi-layer ring-shaped metamaterials for reconfiguration absorbers*", Applied Optics **61**(30), 9078-9084 (2022).

3. The-Linh Pham, Bui Xuan Khuyen, Bui Son Tung, Le Dinh Hai, **Le Van Long**, Vu Dinh Lam and Nguyen Thanh Tung, "*Origami-based stretchable bi-functional metamaterials: reflector and broadband absorber*", Journal of Physics D: Applied Physics **54**, 165111 (2021).

4. **Lê Văn Long**, Dương Thị Hà, Bùi Xuân Khuyến, Nguyễn Thanh Tùng, Bùi Sơn Tùng, Phạm Thanh Sơn, Trịnh Thị Giang, Vũ Đình Lãm, "*Nghiên cứu mô phỏng vật liệu biến hóa có khả năng uốn cong, hấp thụ sóng điện từ trong vùng THz*", Kỷ yếu hội nghị **Những tiến bộ trong vật lý kỹ thuật và ứng dụng VII (CAEP-7),** 7-13, Hà Nội (2022).

5. **Le Van Long,** Bui Son Tung, Bui Xuan Khuyen, Bui Huu Nguyen, Vu Dinh Lam, "*Electrically reconfigurable metamaterial absorber operating in C band*", Journal of Military Science and Technology **91**, 63-72 (2023).